View metadata, citation and similar papers at core.ac.uk
brought to you by CORE
provided by Repository of the Academy's Library

Vacuum 89 (2013) 163-167
http://dx.doi.org/10.1016/j.vacuum.2012.03.049

Growth of ZnO nanostructures on Si by means of plasma immersion ion implantation and deposition

R. M. Oliveira[a *], M. S. Vieira[a], M. Ueda[a], A. Tóth[b]
[a] National Institute for Space Research, São José dos Campos, SP, Brazil
[b] Institute of Materials and Environmental Chemistry, CRC HAS, Budapest, Hungary

Abstract

Crystalline zinc oxide (ZnO) nanostructures have been grown on Si substrates by means of Plasma Based Ion Implantation and Deposition (PIII&D) at temperature of about 300 ^{0}C and in the presence of an argon glow discharge. In the process a crucible filled with small pieces of metallic zinc plays the role of the anode of the discharge itself, being polarized by positive DC voltage of about 400V. Electrons produced by thermionic emission by an oxide cathode (Ba, Sr, Ca)O impact this crucible, causing its heating and vaporization of Zn. Partial ionization of Zn atoms takes place due to collisions with plasma particles. High negative voltage pulses (7 kv/40μs/250Hz) applied to the sample holder cause the implantation of metallic zinc into Si surface, while Zn deposition happens between pulses. After annealing at 700 ^{0}C, strong UV and various visible photoluminescence bands are observed at room temperature, as well as the presence of ZnO nanoparticles. The coated surface was characterized in detail using X-ray diffraction (XRD), X-ray photoelectron spectroscopy (XPS), energy dispersive spectroscopy (EDS), scanning electron microscopy (SEM), atomic force microscopy (AFM) and photoluminescence (PL) spectroscopy. XRD indicated the presence of only ZnO peaks after annealing. The composition analysis by EDS revealed distinct Zn/O stoichiometry relation depending on the conditions of the process. AFM images showed the formation of columns in the nanoscale range. Topography viewed by SEM showed the formation of structures similar to cactus with nanothorns. Depth analysis performed by XPS indicated an increase of concentration of metallic Zn with increasing depth and the exclusive presence of ZnO for outer regions. PIII&D allowed to growing nanostructures of ZnO on Si without the need of a buffer layer.

1. Introduction

Zinc oxide (ZnO) has gathered the attention of the scientific community for many years and it has been the focus of intensive research in various fields due to its significant chemical and physical properties. In fact, in chemical field ZnO is well known as a photocatalyst [1] with high chemical activity, e.g. It is also a singular element with outstanding physical characteristics, being a unique material exhibiting semiconducting and piezoelectric dual properties [2,3]. In addition, a very rich family of ZnO nanostructures, both in structures and in properties [4], can be synthesized under distinct growth methods and conditions [5-8]. Novel potential applications in optoelectronics, transducers, varistors, gas sensors, transparent ultraviolet protection films and biomedical sciences have been demonstrated [9-13]. However, most ZnO nanostructures have been mainly grown on sapphire [14,15], which is rare, expensive and difficult to integrate. When silicon is the substrate, e.g., usually some kind of catalyst or buffer layer must be used [6,16]. Despite the large lattice mismatch between ZnO and Si, which is the main constraint for direct

growth of the film on the substrate [17], some deposition methods can accomplish this task [18,19].

In this paper, crystalline ZnO nanostructures have been grown on Si by means of Plasma Immersion Ion Implantation and Deposition (PIII&D). In a first step metallic Zn is implanted and deposited on Si surface and ZnO nanostructures are attained after annealing in rich oxygen atmosphere. The implantation stage is important to seed the sites for the growth of Zn structures on Si, which will be further oxidized. In fact, the process alternates implantation and deposition. During implantation stage, energetic ions are being implanted in the substrate and also in the deposited film, leading to the formation of an intermixed layer where the substrate material is gradually merged into the film material. So, one of the benefits of PBII&D are the enhanced atomic mixing of film to substrate with the formation of specific crystalline structures [20-22]. The mixed interface region is the responsible for the superior adhesion of the film formed, with reduced stress associated with the structural mismatch of substrate and film material, in comparison with a conventional non-intermixed deposition method.

Notice that unlike conventional ion beam implantation, PIII is a non line-of-sight implantation method [23,24]. It is used for 3D treatments without the need of manipulation of the target and it can open up possibilities for 3D growth of ZnO nanostructures on Si, a substrate for which a mature technological development has been achieved.

2. Experimental

The process of PIII&D was performed in VAST [25,26], acronym for Vaporization of Solid Targets. In this system, showed in Fig. 1, an argon glow discharge is first switched-on at a pressure of 10^{-3} mbar. A molybdenum crucible, which is filled to the top with small pieces of metallic zinc, plays the role of the anode of the discharge itself, being polarized by positive DC voltage at about 200 V. Electrons thermionically produced by an oxide cathode [27] bombard the crucible, causing the vaporization of the zinc at a controlled temperature of 420 ^{0}C. The vapor is partially ionized due to collisions with plasma particles and electrons are drawn from the cathode. Zn ions are implanted into Si when high negative voltage pulses (7 kV/250 Hz/40 μs) are applied to the sample holder. Deposition of neutral Zn takes place between pulses. After PIII&D Si samples were annealed for 1h at 700 ^{0}C in a furnace with flowing oxygen gas under atmospheric pressure.

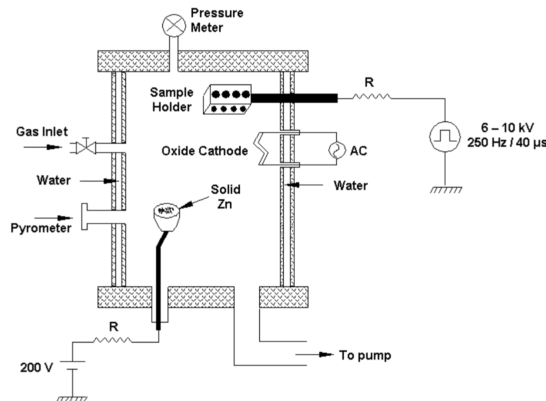

Fig. 1. Experimental apparatus of VAST

The surface morphology of Si was evaluated by means of SEM in a JEOL JSM-5310 apparatus, equipped with EDS, which was used for ZnO stoichiometry analysis. Crystal structure was analyzed by high resolution X-ray diffractometer Phylips X´Pert MRD using Ni filter and operating in the mode of thin films. The surface topography was viewed by AFM images, which was recorded in non-contact mode with a Veeco Multimode and Nanoscope V control station. Qualitative elemental analysis was obtained by XPS measurements performed with a Kratos XSAM 800 spectrometer using Mg $K\alpha_{1,2}$ radiation and fixed analyzer transmission mode (80 and 40 eV pass energies for survey and detailed spectra, respectively) The spectra were referenced to the C 1s line (biding energy, BE = 285.0 eV) of the adventitious hydrocarbon type carbon. Data acquisition and processing were performed with the Kratos Vision 2 program. The PL spectra were acquired using a 325 nm He-Cd laser line as an excitation source at room temperature. Luminescence was detected by monocromator and photomultiplier with the help of a data acquisition system.

3. Results and discussion

Fig. 2 shows high resolution XRD patterns in the as-implanted state (a) and after oxidation at 700^{0}C (b). The sample in the as-implanted state shows distinct diffraction peaks of a mixture of both Zn metal and ZnO, indicating the inhomogeneous nature of the sample. In the diffraction pattern the ZnO (101) peak is dominant and the unique ZnO peak, but other weaker Zn peaks are present. The partial oxidation of Zn in this case is due to residual oxygen present in the vacuum chamber during treatment. In fact, oxygen is usually an impurity always present during PIII, but in this case it played in favor of the oxidation of Zn. The sample after annealing shows a single phase of ZnO. The (101) peak remained as the dominant one, but many other ZnO peaks arose.

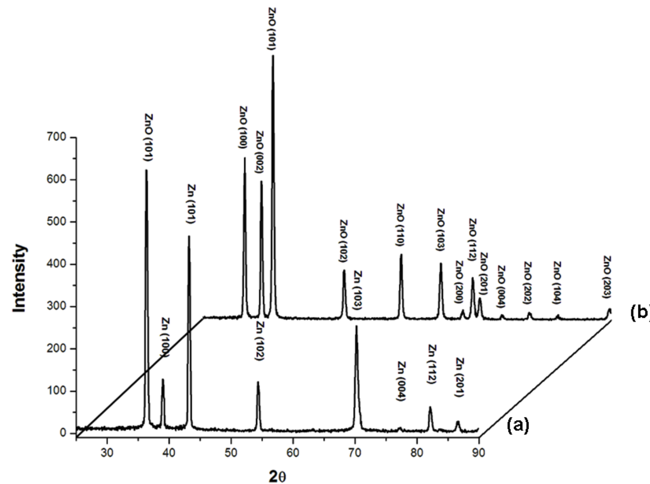

Fig. 2. High resolution XRD performed on Si sample before (a) and after (b) annealing at 700 ^{0}C in rich oxygen atmosphere.

The ZnO stoichiometry analysis was straight determined via software of EDS equipment, by setting the beam energy during measurements to 1 keV. Si substrate was detected only when the beam energy was set above 3 keV. For as-implanted sample (Fig. 3a) the calculated Zn/O

atomic percentage was equivalent to 1.68/1. This relation reached the ideal case of Zn/O = 1/1 after annealing. The increase of the intensity of oxygen peak for this case can be seen in Fig. 3b. It was also observed in previous measurements (results not shown) that annealing temperature plays an important role concerning the oxidation of Zn. For annealing temperature of about 400 ^{0}C there is just a partial oxidation of Zn.

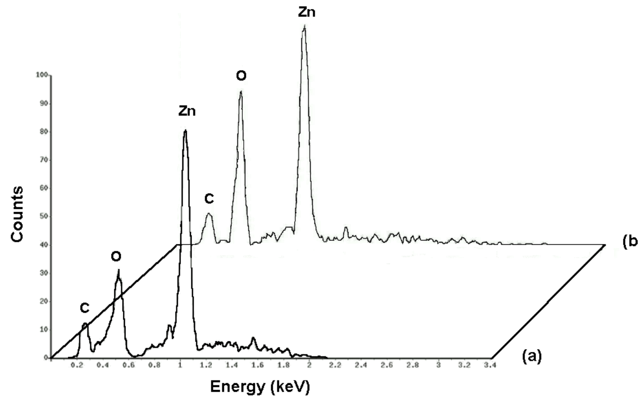

Fig. 3. EDS measurement performed on the as-implanted Si sample before (a) and after annealing (b)

The depth profiles between Zn and ZnO structures for sample submitted to annealing at 400 ^{0}C were determined by Ar^{+} etch profiling using XPS. Ion etch was performed in two steps: 2.5 keV during 15 min (Fig. 4b) and additional 30 min (Fig. 4c). The results at the Zn $L_3M_{45}M_{45}$ transition are shown in Fig. 4.

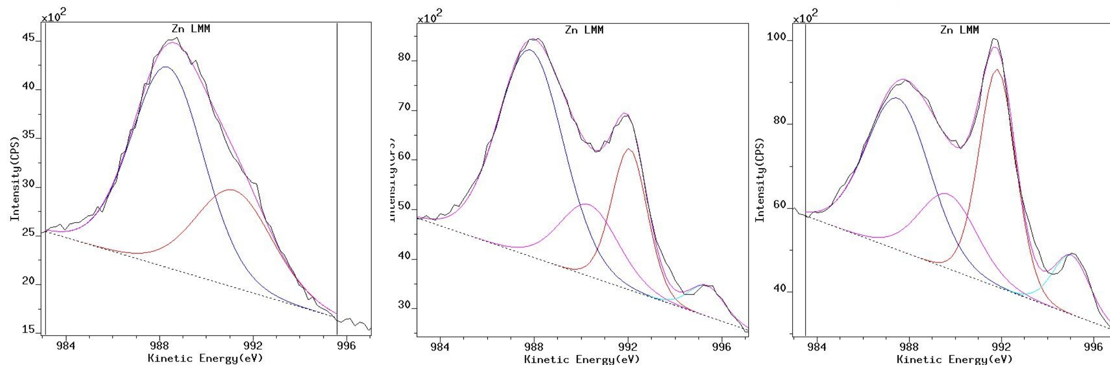

Fig. 4. XPS measurements for determination of depth profiles between Zn and ZnO structures. (a) sputtering time =0 ; (b) after 15 min of sputtering ; (c) after 45 min of sputtering

At the surface (sputtering time = 0 – Fig. 4a), two peaks are present. The dominant one at about 988 eV can be ascribed to ZnO [22] and the other one at about 992 eV is ascribed to metallic Zn. With increasing the etching time the relative intensity of ZnO peak decreases, while the Zn peak increases. Thus, an increase of concentration of metallic Zn with increasing depth can be deduced. ZnO sputters congruently, that is without change in the stoichiometry, therefore the increase of metallic Zn with increasing depth should be a real effect. The role played by Zn implantation in the beginning of the process is necessary to form a conducting intermixing layer. However, in PBII&D, when the growing film is thicker than the implantation depth, ion

implantation does not contribute anymore to the intermixing but is still essential to the structure of the film.

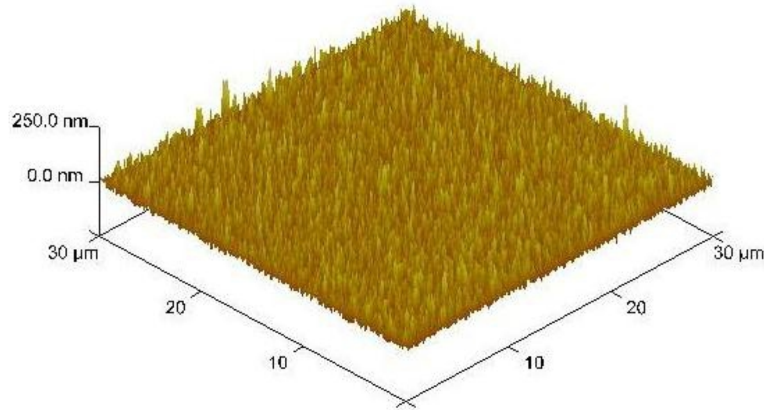

Fig. 5. 3D AFM image of as-implanted sample

A 3D AFM image of the film surface of the as-implanted sample is shown in Fig. 5. The scanning area was a square of 30 µm side. Average roughness measured was about 22.9 nm while average height of the structures, similar to columns, was of 90 nm. The topography of the samples after being annealed could not be viewed in this case because of limitations of the AFM to examine nanostructures.

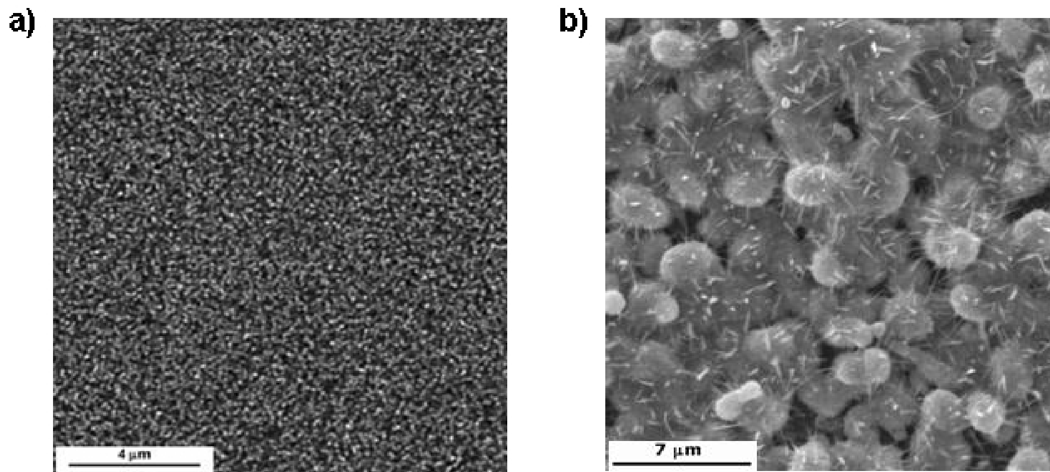

Fig. 6. SEM images for as-implanted sample (a) and after annealing (b)

Fig. 6a shows scanning electron microscopy image corresponding to the sample which AFM image was shown in Fig. 5. It can be observed regular uniformity of the grown film. The mean crystallite size measured is about 82 nm. After annealing at 700 ^{0}C in rich oxygen atmosphere the sample presented significant change of superficial morphology, as can be seen in Fig. 6b. Microstructures resembling microcactus and nanothorns with random orientation can be observed. Changes on the morphology of grown ZnO films after annealing at different temperature range were extensively discussed on the literature [28-30].

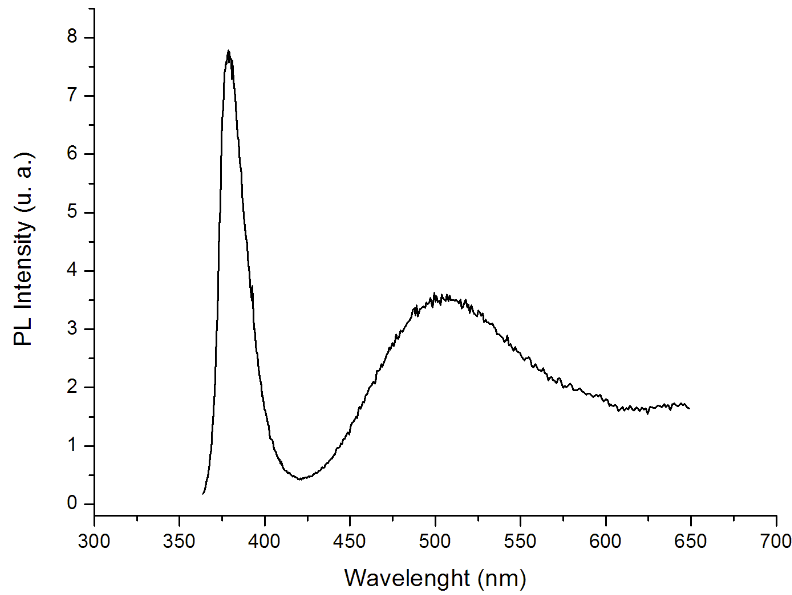

Fig. 7. Photoluminescence spectrum of ZnO nanostructures

The photoluminescence spectrum of ZnO nanostructures attained after annealing at 700 ^{0}C is shown in Fig. 7. Narrow and intense UV band at 380 nm in wavelength and a broad green band with peak at 504 nm are observed in the photoluminescence spectrum of Fig. 7a. On the other hand, distinct spectra are attained in VAST by performing IIIP in discharges mixing argon and oxygen. Usually, as high the oxygen content during the process, more intense green peaks are attained. A typical case is the result shown in Fig. 7b.

The UV emission band of wide band gap ZnO nanostructures is explained by the recombination of free excitons through an exciton-exciton collision process [31]. The green band emission is still controverse, but, to the best of our knowledge, it results from the recombination of a photogenerated hole with an electron that belongs to a singly ionized oxygen vacancy [32].

4. Summary

Crystalline ZnO nanostructures were grown on silicon substrate without the need of a catalyst or buffer layer, using PIII&D. The implantation of Zn ions previously to the deposition allows a straight growth of ZnO on Si surface. The process runs in low temperature and its operation parameters are easily controlled. The samples were characterized by EDS, XRD, AFM, XPS, SEM and PL spectroscopy, in order to infer their stoichiometry, phase characterization, topography, qualitative elemental analysis, morphology and photoluminescence emission, respectively. Post-oxidation stage was demanded to the achievement of the nanostructures and emission of intense photoluminescence at room temperature.

References

[1] Takai O, Futsuhara M, Shimizu G, Lungu CP, Nozue J. Thin Solid Films 1998;318:117.
[2] Jagadish C, Pearton SJ. Zinc oxide bulk, thin films and nanostructures. 1st ed. Hong Kong: Elsevier; 2006.
[3] Wang LZ. J Phy Cond Mat 2004;16:829.
[4] Fang ZB, Yan ZJ, Tan YJ, Liu XQ, Wang YY. App Surf Sci 2005;241:303.
[5] Li ZW, Gao W. Thin Solid Films 2007;515:3323.
[6] Lee CY, Tseng TY, Li SY, Lin P. Tamkang J Sci Eng 2003;6(2):127.
[7] Lee A, Jeong S, Kim D, Hwang S, Jeon M, Moon J. Superl Micro 2008;43:330.
[8] Huang MH, Wu Y, Feick H, Tran N, Weber E, Yang P. Adv Mater 2001;13(2):113.
[9] Lupan O, Chai G, Chow L. Novel Microelec Eng 2008;85:2220.
[10] Wary G, Kachary T, Rahman A. Inter J Therm 2006;27(1):332.
[11] Wongchoosuk C, Choopun S, Tuantranont A, Kerdcharoen T. Mat Res 2009;9(3):185.
[12] Hsiao Chun-Ching, Huang Kuo-Yi, Hu Yuh-Chung. Sensors 2008;8:185.
[13] Wu W, Bai S, Cui N, Ma F, Wei Z, Qin Y, et al. Sci Adv Mat 2010;2:402.
[14] Özgür Ü, Alivov YI, Liu C, Teke A, Reshchikov MA, Dogan S, et al. J App Phy 2005;98.
[15] Wei XQ, Man BY, Liu M, Xue CS, Zhuang HZ, Yang C. Phy B 2007;388:145.
[16] Wang DD, Yang JH, Yang LL, Zhang YJ, Lang JH, Gao M. Cryst Res Technol 2008;43(10):1041.
[17] Joseph M, Tabata H, Kawai T. Appl Phys Lett 1999;74(17):2534.
[18] Ogata K, Kim S-W, Fujita Sz, Fujita Sg. J Crystal Growth 2002;240:112-6.
[19] Lupan O, Pauporté T, Ursaki VV, Tiginyanu IM. Opt Mater 2011;33:914-9.
[20] Pelletier J, Anders A. Plasma-based ion implantation and deposition: a review of physics, technology, and applications. Lawrence Berkeley National Laboratory. pp. 1-68, http://escholarship.org/uc/item/84k974r2; 2005.
[21] Anders A, Anders S, Brown IG, Dickinson MR, MacGill RA. J Vac Sci Technol B 1994;12(2):815.
[22] Amekura H, Umeda N, Yoshitake M, Kono K, Kishimoto N, Buchal Ch. J Cryst Growth 2006;287:2.
[23] Anders A. Handbook of plasma immersion ion implantation and deposition. 1st ed. Canada: John Wiley & Sons; 2000. p. 736.
[24] Conrad JA. Mat Sci Eng A 1989;116:197.
[25] Oliveira RM, Gonçalves JAN, Ueda M, Oswald S, Baldissera SC. Surf Coatings Technol 2010;204:2981-5.
[26] Oliveira RM, Ueda M, Rossi JO, Diaz B, Baba K. IEEE Trans Plasma Sci 2008;36: 2572-6.
[27] Gonçalves JAN, Sandonato GM, Neto CM. Vacuum 1998;49:9-15.
[28] Lai LW, Lee CT. Mat Chem Phy 2008;110:393-6.
[29] Sharma S, Sehrawat K, Wakahara A, Mehra RM. App Sur Sci 2009;255: 5781.
[30] Zhang Y, Du G, Yang X, Zhao B, Ma Y, Yang T, et al. Semic Sci Tech 2004;6:755.
[31] Kong YC, Yu DP, Zhang B, Fang W, Feng SQ. Appl Phys Lett 2001;78:407.
[32] Vanheusden K, Warren WL, Seager CH, Tallant DK, Voigt JA, Gnade BE. J Appl Phys 1996;79:7983.